Direct Phasing in Electron Crystallography: Ab Initio Determination of a New MCM-22 Zeolite Structure

S. Nicolopoulos,[†,‡] J. M. González-Calbet,[*,†] M. Vallet-Regí,[‡] A. Corma,[§] C. Corell,[§] J. M. Guil,[⊥] and J. Pérez-Pariente[∥]

Contribution from the Departamento de Química Inorgánica, Facultad de Químicas, Universidad Complutense, 28040 Madrid, Spain, Departamento de Química Inorgánica y Bioinorgánica, Facultad de Farmacia, Universidad Complutense, 28040 Madrid, Spain, Instituto de Tecnología Química, Universidad Politécnica de Valencia, UPV-CSIC, 47061 Valencia, Spain, Instituto de Química Física, CSIC, Serrano, 119, 28006 Madrid, Spain, and Instituto de Catálisis y Petroleoquímica, CSIC, Campus Universidad Autónoma, Cantoblanco, 28049 Madrid, Spain

Received November 14, 1994. Revised Manuscript Received March 6, 1995[⊗]

Abstract: Experimental electron diffraction intensity data from a new MCM-22 zeolite have been used for a direct structure determination based on probabilistic estimates of triple invariant sums. It is known from previous catalytic measurements that the MCM-22 structure contains large intersecting channels of 12- and 10-member rings. By using electron microdiffraction and direct method procedures (method of averages and distribution method) the space group is assigned to *P6/mmm*. Direct phasing of (*hki*0) reflections leads to a (0001) potential E-map where the large channel of the 12-fold ring and the basal framework topology are clearly resolved. On the other hand, on the resultant ($11\bar{2}0$) E-map obtained after direct phasing of (000*l*) reflections a sinusoidal modulation of the large 12-fold ring channel parallel to the *c*-axis is inferred.

Introduction

Zeolites are microporous materials largely used in adsorption and catalytic processes, owing to their molecular sieve characteristics. It can be of great interest for industrial use to produce zeolite catalysts that contain channels of 12- and 10-member rings. Such zeolites could combine in only one structure the ability of large pores to convert heavy molecules with the shape selectivity of medium pore zeolites. Recently, a new zeolite named MCM-22 has been synthesized and patented.[1] Catalytic tests indicated that MCM-22 contained voids formed of 10- and 12-member rings.[2−4] Later on, Leonowicz et al.[5] analyzed high resolution electron micrographs together with synchrotron X ray diffraction powder data refinement and proposed that the zeolite is composed of interconnected $\{4^35^66^3[4^3]\}$ building units forming a dodecasil-1-H-like crystal lattice belonging to the *P6/mmm* or *Cmmm* space group. The structural models contain two independent multidimensional channel systems with the largest rings of 10 and 12 tetrahedral atoms. The largest pore has a diameter of 0.71 nm and its height is 1.82 nm. Finally, an electron diffraction study we performed[6] has shown the unit cell parameters and the point group symmetry of this new zeolite; the cell parameters of this compound were further reconfirmed in a later study.[7]

Recent work by Dorset[8−17] and previous pioneering work by Cowley[18] and Russian crystallographers[19−25] has proved the possibility of crystal structure determination by electron diffraction. It is worth mentioning that electron crystallography, which combines information from several views of a crystal, has been directly employed to solve the crystal structure of staurolite, a complex aluminosilicate mineral;[26] such results being in agreement to those obtained by X-ray crystallography.

* To whom correspondence should be addressed.
[†] Departamento de Química Inorgánica, Facultad de Químicas, Universidad Complutense.
[‡] Departamento de Química Inorgánica y Bioinorgánica, Facultad de Farmacia, Universidad Complutense.
[§] Instituto de Tecnología Química, Universidad Politécnica de Valencia.
[⊥] Instituto de Química Física.
[∥] Instituto de Catálisis y Petroleoquímica.
[⊗] Abstract published in *Advance ACS Abstracts*, August 1, 1995.

(1) U.S. Patent, 5, 085, 762, 1992.
(2) Corma, A.; Corell, C.; Pérez-Pariente, J.; Guil, J. M.; Guil-Lopez, R.; Nicolopoulos, S.; González-Calbet, J. M.; Vallet-Regí, M. *Zeolites* **1995**, in press.
(3) Corma, A.; Corell, C.; LLopis, F.; Martínez, A.; Pérez-Pariente, J. *Appl. Catal.* A **1994**, *115*, 121−125.
(4) Souverijns, W.; Verreist, W.; Vanbutsele, G.; Martens, J. A.; Jacobs, P. A. *J. Chem. Commun.* **1994**, 1671−1675.
(5) Leonowicz, M. E.; Lawton, J. A.; Lawton, S. L.; Rubin, M. K. *Science* **1994**, *264*, 1910−1913.
(6) Nicolopoulos, S.; Corma, A.; Corell, C.; Pérez-Pariente, J.; Vallet-Regí, M.; González-Calbet, J. M. in *Proceedings of the 13th International Congress on Electron Microscopy ICEM-13*, Paris, **1994**, pp 823−824.
(7) Chan, I. Y.; Labun P. A.; Pan M.; Jones S. I. *Microporous Mater.* **1995**, *3*, 409−418.
(8) Dorset, D. L. *Ultramicroscopy* **1991**, *38*, 23−40.
(9) Dorset, D. L. *Acta Crystallogr.* **1992**, *A48*, 568−574.
(10) Dorset, D. L. *Ultramicroscopy* **1992**, *45*, 5−14.
(11) Dorset, D. L. *Ultramicroscopy* **1992**, *45*, 357−364.
(12) Dorset, D. L.; McCourt, M. P. *J. Struct. Biol.* **1993**, *111*, 118−124.
(13) Dorset, D. L.; McCourt, M. P.; Tivol, W. F.; Turner, J. N. *J. Appl. Crystallogr.* **1993**, *26*, 778−786.
(14) Dorset, D. L.; McCourt, M. P. *Acta Crystallogr.* **1994**, *A50*, 344−351.
(15) Dorset, D. L. *J. Chem. Crystallogr.* **1994**, *24*(3), 219−224.
(16) Dorset, D. L. *Advances in Electronics and Electron Physics*; Academic Press: New York, 1994; Vol. 88, pp 111−197.
(17) Dorset, D. L.; Zhang, W. J. *Electron Microsc. Technique* **1991**, 142−147.
(18) Cowley, J. M. *Acta Crystallogr.* **1953**, *6*, 522−529.
(19) Vainstein, B. K. *Structure Analysis by Electron Diffraction*; Pergamon Press: Oxford, 1964.
(20) Vainstein, B. K. *Zh. Fiz. Khim.* **1955**, *29*, 327−344.
(21) Lobachev, A. N.; Vainstein, B. K. *Sov. Phys. Crystallogr.* **1961**, *6*, 313−316.
(22) Zvyagin, B. B. *Electron Diffraction Analysis of Clay Mineral Structure*; Plenum: New York, 1967.
(23) Zvyagin, B. B.; Mischenko, K. S. *Sov. Phys. Crystallogr.* **1961**, *5*, 575−579.
(24) Zvyagin, B. B. *Sov. Phys. Crystallogr.* **1957**, *2*, 388−394.
(25) Zvyagin, B. B.; Mischenko, K. S. *Sov. Phys. Crystallogr.* **1963**, *7*, 502−505.
(26) Downing, K. K.; Meisheng, H.; Wenk, H. R.; O'Keefe, M. A. *Nature* **1990**, *6*, 525−528.

0002-7863/95/1517-8947$09.00/0

Moreover, oxygen atoms could be clearly identified in the final Fourier map (called potential maps in electron crystallography) which also contains heavy atoms such as aluminium, silicon, and iron.

An extensive literature on the early crystal structure analysis using electron diffraction intensities on many-layer silicate structures has been summarized by Zvyagin.[22-25] In this early work, electron crystallography has been used to built models of expected layer packing, oxygen positions being also visualized in the final potential maps.

Electron crystallography techniques have also been applied to solve a number of structures (organic compounds, polymers, etc.), the results being consistent with previous X-ray investigations on these materials and demonstrating the potential of the method to resolve ab initio structures of crystals too small for X-ray techniques.

Nevertheless, despite the very promising results (e.g., on silicate structures and aluminosilicate minerals) electron crystallography techniques have never been used—as far as we know—to resolve zeolite structures. Therefore, it seems interesting to apply this technique to confirm the previously proposed symmetry[6,7] and to proceed to an ab initio crystal structure determination of the MCM-22 structure. Moreover, as will be shown below, the proposed model by synchrotron X-ray diffraction data[5] served us to check for the validity of the electron crystallography techniques to the ab initio analysis for the MCM-22 zeolite.

Direct Phasing Methods in Electron Crystallography

During the last few years, the term "electron crystallography" has been used to denote the quantitative crystal structure determination based on electron diffraction intensity data and/or high resolution electron microscopy images. This technique, similar to X-ray crystallography, requires the same sort of procedures for finding crystallographic phases to derive a potential map with crystal structure details.

Early works on structure analysis by electron diffraction mostly relied on various trial and error approaches or interpreting Patterson functions.[22-25] However, the so-called "direct phasing methods", based on probabilistic estimates (this term will be explained below) of structure invariant sums,[27] have been recently found very useful for ab initio crystal structure determination based on electron diffraction intensities.[8-17] In fact, traditional direct methods in X-ray crystallography may also be used in electron crystallography.

Hence, when only electron diffraction intensity data are available for an ab initio determination of crystallographic phases, probabilistic estimates of a linear combination of phases, as in X-ray crystallography,[27] of the type $\phi = \phi_{h1} + \phi_{h2} + \phi_{h3} + \ldots$ can be very useful if they have the constraint that the Miller index sum is $\sum \boldsymbol{h}_i = \sum h_i k_i l_i = 0,0,0$. In that case, this sum of phases is known as a structure invariant, i.e., it is true no matter where the unit cell origin is defined. If there are three phases in this invariant, it is known as "triple invariant". If $\mathbf{h}_1 \neq \mathbf{h}_2 \neq \mathbf{h}_3$, it is known as Σ_2 triple, and if $\mathbf{h}_1 = \mathbf{h}_2 = -\mathbf{h}_3/2$, one defines a Σ_1 triple. Therefore, for any electron diffraction reflection with Miller index values $\mathbf{h}_i$, it is possible to generate arbitrarily a number of structure invariants which are, in fact, a list of simultaneous equations where crystallographic phases are the unknowns. As long as it is also possible to evaluate the probability of being correctly predicted, these simultaneous equations can be ranked from most to least probable (probabilistic estimate).

For Σ_2 triplets, the probability of $\phi = 0$ is based on the magnitude of $A_2 = (2/\sqrt{N})|E_{h1}E_{h2}E_{h3}|$ (for an equal atom case with N representing the number of atoms in the unit cell). For Σ_1 triplets, the likehood of $\phi = \pi$ can be estimated from large negative values of $A_1 = (|E_h|^2 - 1)E_{2h}/\sqrt{N}$. Otherwise, large positive values of A_1 indicate ϕ_{2h} near 0. (The meaning of normalized structure factor magnitudes E_h will be explained below.)

It is worth realizing that the different phase invariant sums (e.g., Σ_1 and Σ_2 triples) can be ranked in their probabilistic order of being correctly determined. Hence, not only do we have simultaneous equations in phase, but they can also be ranked in order of their reliability.

As we can observe, the probability of the structure invariant sum being correctly predicted is related, in all cases, to the magnitude of the normalized structure factor, defined as

$$|E_h|^2 = |F_h|^2/\epsilon\sum f_i^2 \qquad (1)$$

where F_h are the observed structure factor magnitudes, f_i are the electron scattering factor values,[28] and ϵ is a multiplicity factor to correct zones with systematic absences.

These structure factors $|E_h|$ are normalized so that $\langle|E|^2\rangle = 1.000$. Indeed, this is not strictly correct for limited electron diffraction data sets, but for most purposes, the approximation seems to be sufficiently accurate to permit ab initio structure analysis to be realized. Ideally, E_h is a structure factor for point atoms at rest. Hence, an overall temperature factor B_{iso} may be estimated for the molecule; this can be done after a Wilson plot[29] of the experimental data:

$$\ln\langle I_h^{obs}/\sum F_h^2\rangle = \ln C - 2B_{iso}(\sin^2\theta/\lambda^2) \qquad (2)$$

A plot of $\ln\langle I_h^{obs}/\sum F_h^2\rangle$ *vs* an average value of $\sin^2\theta/\lambda^2$ for succesive shells of reciprocal space will determine the temperature factor B_{iso}. Once the E_h values are calculated, these are ranked in decreasing magnitude and the values of certain averages of these magnitudes are compared to theoretical values expected for centrosymmetric (**cs**) or non centrosymmetric structures (**ncs**)[30] as will be shown below.

Now, to proceed to the crystal structure determination, we must be able to obtain a small set of starting phase values, being possible, in that case, to solve most probable simultaneous Σ_1 and Σ_2 triples equations to determine enough new phase values ϕ_h to allow an interpretable potential map (i.e., where some or all atomic positions can be clearly depicted) to be calculated from

$$\varrho(r) = V^{-1}\sum|F_o|\exp(i\phi_h)\exp[-2\pi i(hx + ky + lz)] \qquad (3)$$

which is a partial reverse Fourier transform based on a limited phase set.

It is possible that a few invariant Σ_1 and Σ_2 phase sums may be incorrectly predicted, leading either to false phase assignments or at least to phase assignments inconsistent with those found from other Σ_1 and Σ_2 invariants. A small number of such errors can generally be tolerated.[10,15,16]

It is important to emphasize that, given the initial set of strong phase values, one works through the invariant sums algebraically to find the values of other phases. If this evaluation goes well, then enough phase values are found to calculate an interpretable potential map. If not enough phase values are assigned, then

(27) Hauptman, H. A. *Crystal structure determination: The Role of cosine seminvariants*; Plenum: New York, 1972).

(28) Doyle, P. A.; Turner, P. S. *Acta Crystallogr.* **1968**, *A24*, 390–397.

(29) Wilson, A. J. C. *Nature* **1942**, *150*, 151–152.

(30) Giacovazzo, C. *Direct Methods in Crystallography*; Academic Press: London, 1980.

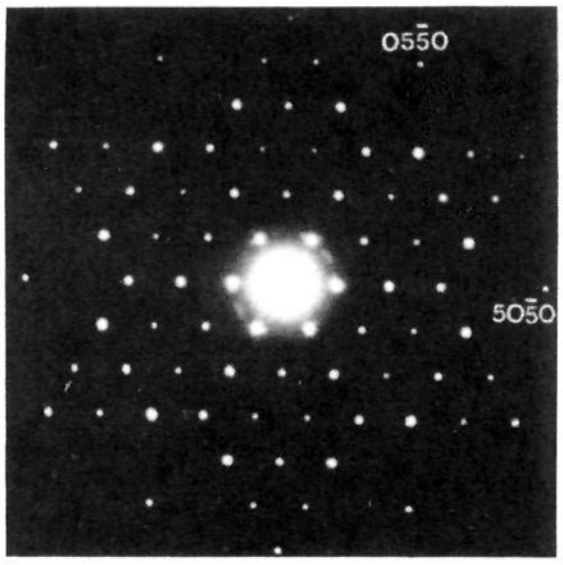

Figure 1. SAED pattern of MCM-22 zeolite along [0001].

algebraic quantities can be used to determine relative phase relationships among a group of reflections.

If $n = a, b, c, ...$, algebraic unknowns are used to establish phase linkage among certain reflections and then enough reflections are given at least symbolic phase assignment (e.g., $\phi_{hkl} = a, b, c, ...$), 2^n potential maps will be calculated (since $a = 0, \pi$; $b = 0, \pi$; etc, for **cs** structures), and the correct structure will be identified by inspection of the potential maps (e.g., with chemical knowledge of the molecular geometry).

Experimental Section

Materials. MCM-22 was synthesized using haxamethyleneimine (HM) as a template following the procedure described in ref 1. Crystallization of the gels was done in Teflon-lined stainless steel autoclaves at 408 K for 9 days under rotation at 60 rpm. After the synthesis, the autoclaves were cooled down to room temperature, and the solids were washed with deionized water until pH 9. After drying at 353 K, the sample was calcined at 853 K for 3 h. The position and intensity of the X-ray diffraction (XRD) peaks (Figure 1) agree with those given in ref 1 for a MCM-22 sample.

Instrumentation. Powder XRD data were performed on a Phillips 1060 diffractometer provided with graphite monocromator and using Ni-filtered Cu Kα radiation ($\lambda = 0.1542$ nm). Crystal size and shape were determined by scanning electron microscopy (SEM) on a ISI DS 130 apparatus. Transmission electron microscopy (TEM) observations were performed on a JEOL 2000FX microscope operated at 200 kV and equipped with a side entry specimen holder. A PDS microdensitometer (Perkin Elmer model 1010M) was used for evaluation of the electron diffraction intensities.

Results

Electron Diffraction and Microscopy Study. A. Unit Cell and Point Group Symmetry Determination. According to early results,[6] the selected area electron diffraction (SAED) pattern of MCM-22 zeolite along [0001] (Figure 1) suggests a hexagonal unit cell with parameters $a = b = 1.43$ nm. All synthesized crystals are highly textured platelet forms and with the c axis as a texture axis.[18] On the basis of SAED patterns, a value of $c = 2.64$ nm is obtained.

Powder XRD data (Figure 2) are consistent with the hexagonal cell proposed, but the rather strong angular width of the X-ray maxima indicates a small crystallite size or/and a quite faulted structure. According to SEM micrographs,[2] the average crystal size can be estimated as between 100 and 200 nm, having a thickness of around 30 nm. On the other hand, the streaking observed along the c axis (Figure 3) suggests some kind of disorder in stacking along the [0001] direction. Variations of the a parameter ($\leq 3\%$) detected in SAED patterns over several examined crystals also indicate that the synthesized material seems to be faulted to some extent.

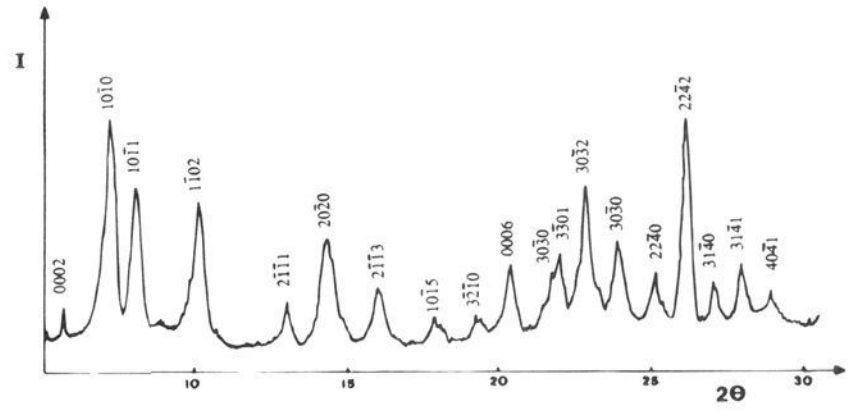

Figure 2. XRD pattern of the MCM-22 zeolite.

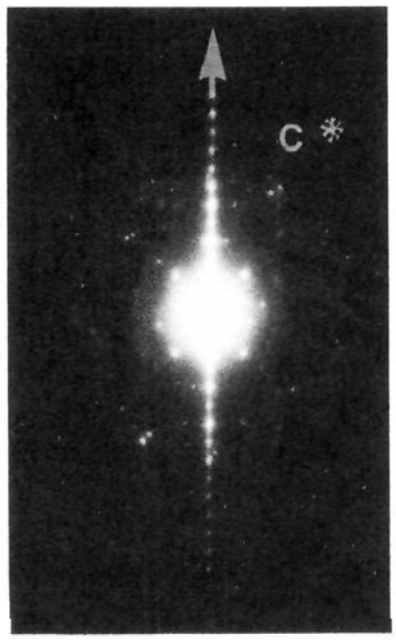

Figure 3. Systematic (000l) row of the MCM-22 structure showing the existence of streaking along the c^* axis.

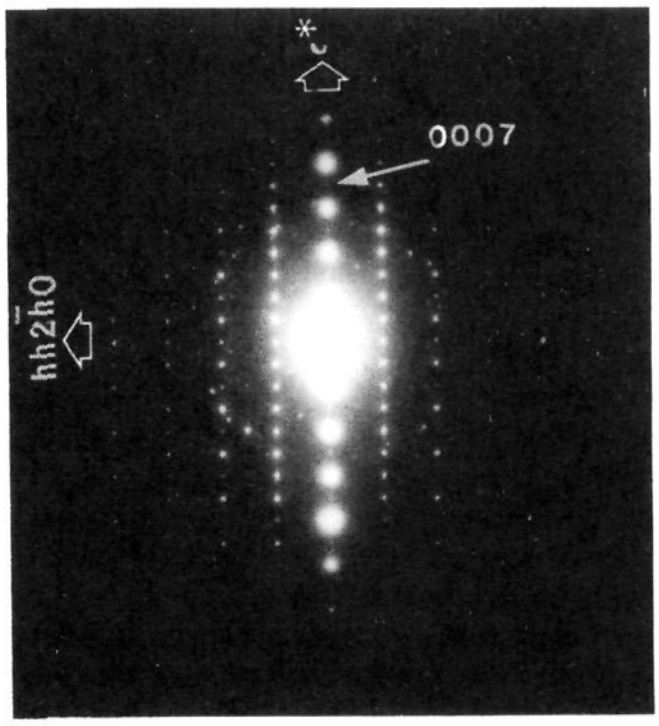

Figure 4. Microdiffraction pattern along [1$\bar{1}$00]; (2*mm*) ideal ZOLZ symmetry is observed.

From the direct comparison of both Figures 3 and 4 it can be observed that the intensity of various reflections, e.g., (0002), (0004), etc., ..., seems to vary with crystal tilt, inferring the existence of dynamical diffraction.[31] As a consequence, and since secondary scattering and possible structural disorder may affect the appearance of some forbidden reflections, space group determination based on extinctions in SAED patterns is not reliable in this case. As a possible solution to this problem, the symmetry of microdiffraction patterns can yield information from small areas of the sample and may be used for point group

(31) Cowley, J. M.; Kuwabara, S. *Acta Crystallogr.* **1962**, *15*, 260–270.

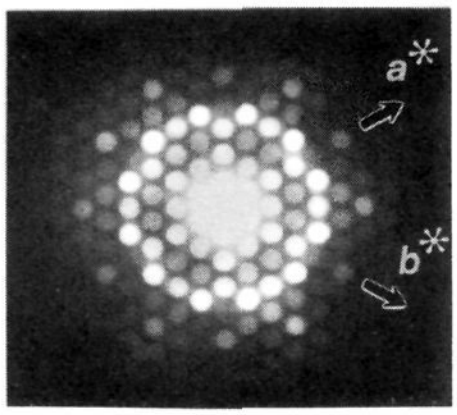

Figure 5. Microdiffraction pattern along [0001]; (6*mm*) ideal ZOLZ symmetry is observed.

symmetry determination.[32] Microdiffraction technique may be used as an alternative tool to convergent beam (CBED) patterns giving distorted details within the transmitted and diffracted disks, as occurs in our case, probably because of quick radiation damage and (or) crystal faulting at a nanometric level which severely distorts details within the observed CBED discs, although dynamical interactions may be important.

By choosing the smallest condenser aperture and working at 80 kV, a microdiffraction pattern along [0001] was obtained (Figure 5). It is worth recalling that due to the high instability under the electron beam of zeolite materials, such information is very rarely obtained. This pattern shows a (6*mm*) "ideal" symmetry according to the terminology used in ref 32 in the zero order Laue zone (ZOLZ). Moreover, the presence of (2*mm*) ZOLZ "ideal" symmetry in the microdiffraction pattern along [$1\bar{1}00$] (Figure 4) and along [$2\bar{1}\bar{1}0$] indicates that the crystal has hexagonal symmetry with possible point groups 6/*mmm* or 622. Both groups have *p*6*mm* projection plane symmetry along the [0001] orientation.[33]

B. Electron Microscopy Observations. Figure 6a shows an electron micrograph of the MCM-22 zeolite along [0001], with the inset optical diffractogram. This image is similar to that of zeolite L along [0001].[34] As long as the [0001] projection of the two structures is similar (concerning the size of the 12-member ring pore system), it is possible to assume that, according to image simulations performed in zeolite L,[34] large white dots do coincide with the main 12-ring channels. Nevertheless, the image characteristic of the MCM-22 zeolite changes notoriously with the amount of defocus (Figure 6b). Therefore, it seems that image simulation experiments performed for a large range of focus are needed to confirm the possible analogy with zeolite L.

Figure 7 shows a micrograph with the [0001] incidence. In part A, the associated inset optical diffractogram reveals the 6-fold symmetry of this domain, arrowed boundaries indicating that the structure is faulted at a nanometric level. Those boundaries separate different overlapping crystallites rotated by 30° with respect to one another around the *c* axis, as can be shown from the corresponding optical diffractogram in part B having a 12-fold symmetry. This relative rotation of 30° between two different domains can also be seen in the left part of Figure 7. Such a rotation leads to Moiré patterns as in the case of zeolite L. White "rings" of 12-fold symmetry are clearly seen within those hexagonal Moiré patterns (Figure 7 bottom inset). As shown by Terasaki et al.[34] in the case of zeolite L, such rotational Moiré patterns may enhance and, indirectly, resolve the projected zeolite framework topology, otherwise

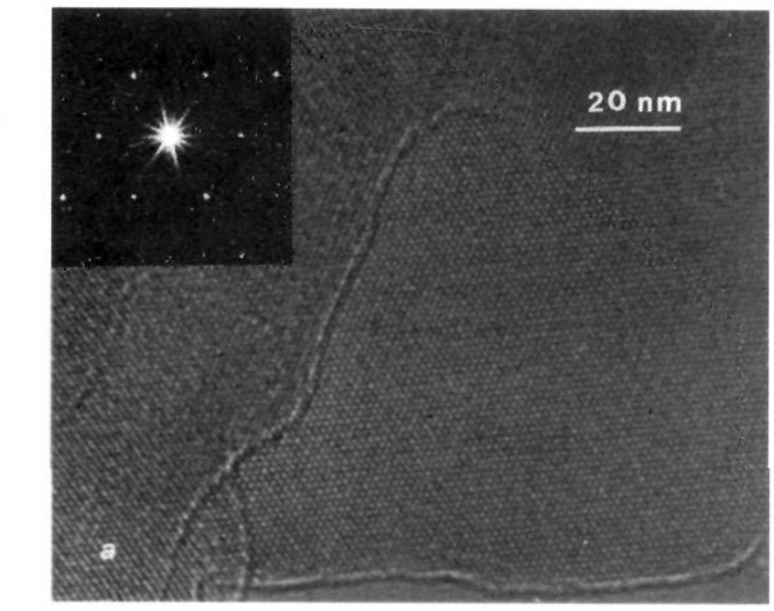

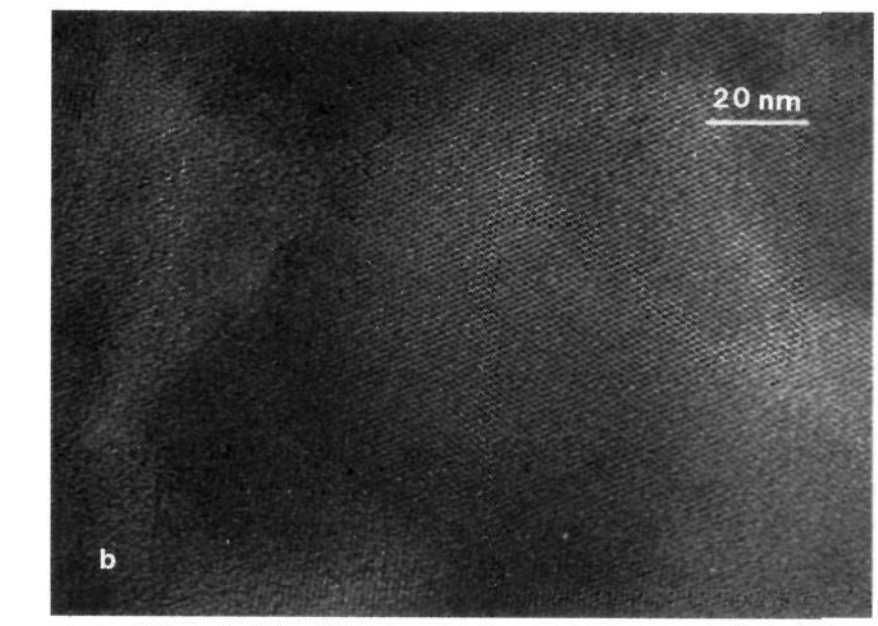

Figure 6. (a) [0001] electron micrograph of MCM-22 zeolite. Inset: optical diffraction of the micrograph. (b) Electron micrograph along [0001] showing different image contrast from (a) at different defocus values.

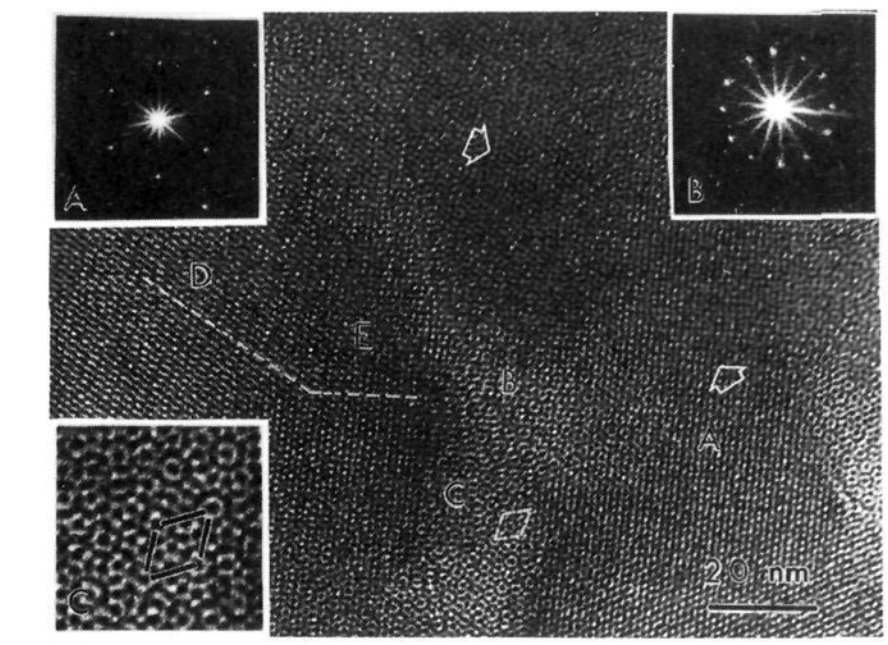

Figure 7. Electron micrograph along [0001] showing superimposed crystals. Top inset: optical diffraction from regions A and B. Bottom inset: enlarged image of the Moiré pattern shown in region C. The relative rotation of 30° between the domains D and E is delineated.

hardly interpretable in domains where crystals do not overlap (see area A in Figure 7).

Nevertheless, even if some similarity is assumed between the [0001] projected crystal structure of zeolite L and the MCM-22 zeolite, the straightforward interpretation of the Moiré pattern (see Figure 7, bottom inset) in terms of projected framework topology of the MCM-22 zeolite is quite fortuitous. We shall later deal with this important point in the discussion section.

(32) Mornirolli, J. P.; Steeds, J. W. *Ultramicroscopy* **1992**, *45*, 219–239.

(33) *International Tables for Crystallography*; Kluwer Academic Publishers: Dordrecht, The Netherlands, 1989; Vol. A.

(34) Terasaki, O.; Thomas, J. M.; Millward, G. R. *Proc. R. Soc. London* **1984**, *A395*, 15, 153–164.

Table 1. Statistical Characteristics of Rhombohedral and Hexagonal Crystal Classes[30,41]

crystal class	centric sets
$3m(1)$	$\{h0\bar{h}0\}$
$32(1)$	$\{h0\bar{h}l\}$
$\bar{3}m(1)$	all
$\underline{6}$	$(hki0)$
$\bar{6}$	$(000l)$
$6/m$	all
$\bar{6}m2$	$[\{hh2\bar{h}l\}; \{hh2\bar{h}0\}; (000l)]$
$6mm$	$[(hki0); \{hh2\bar{h}0\}; \{h0\bar{h}0\}]$
62	$(hki0); (h0\bar{h}l); (hh2\bar{h}l)$
$6/mmm$	all

Table 2. Distribution of $|E_h|$ Values for Representative Electron Diffraction Data Sets

	theory		experimental				
	noncentro-symmetric	centro-symmetric	$hki0$	$hh2\bar{h}l$	$000l$	$h0\bar{h}0$	$hh2\bar{h}0$
(a) Dynamical Assumption ($\|F_h\| \propto I_h$)							
$\langle\|E_h\|^2\rangle$	1.0	1.0	1.0	1.0	1.0	1.0	1.0
$\langle\|E_h\|\rangle$	0.886	0.798	0.715	0.64	0.564	0.780	0.684
$\langle\|E_h^2 - 1\|\rangle$	0.736	0.968	1.147	1.346	1.361	0.931	1.177
% $\|E_h\| > 1$	36.8	32.0	21.9	30.7	28.5	44.4	40.0
% $\|E_h\| > 2$	1.8	5.0	2.7	11.5	14.3	11.1	0.0
% $\|E_h\| > 3$	0.01	0.3	2.7	0.0	0.0	0.0	0.0
(b) Kinematical Assumption ($\|F_h\| \propto I_h^{1/2}$)							
$\langle\|E_h\|^2\rangle$	1.0	1.0	1.0	1.0	1.0	1.0	1.0
$\langle\|E_h\|\rangle$	0.886	0.798	0.906	0.837	0.678	0.903	0.804
$\langle\|E_h^2 - 1\|\rangle$	0.736	0.968	0.651	0.841	1.23	0.635	1.036
% $\|E_h\| > 1$	36.8	32.0	37.8	26.92	28.57	22.22	40.0
% $\|E_h\| > 2$	1.8	5.0	0.0	0.0	0.0	0.0	0.0
% $\|E_h\| > 3$	0.01	0.3	0.0	0.0	0.0	0.0	0.0

On the other hand, the image features within the hexagonal Moiré pattern (Figure 7, bottom inset) seem to be related by a *p6mm* projection symmetry, the corresponding optical diffraction pattern of the Moiré supercell having 12-fold symmetry (Figure 7, top right inset). The above data agree with the proposed *p6mm* projected point group symmetry for the MCM-22 framework topology since the relative rotation by 30° of two MCM-22 crystallites apparently conserves the *p6mm* symmetry in the resulting interference Moiré pattern.

Structure Analysis by Electron Diffraction. A. Assignment of the Point and Space Group Symmetry by Direct Methods. As we have seen in the previous section, the possible point group symmetry deduced from microdiffraction has proved to be either *6/mmm* or 622. In order to distinguish between them, we have used the "distribution method" and the "method of averages", as established by Rogers and Wilson.[35-37]

According to the "distribution method", different crystal classes could be distinguished from examination of the intensity distribution (see Table 1). The theoretical probability distribution of structure factors was first derived by Wilson[36] under the hypothesis that the atomic positions are random variables with uniform distribution throughout the unit cell (i.e., all points in the cell have the same probability of hosting an atom). Their form depends on whether the crystal possesses (centric distribution) an inversion center or not (acentric distribution).

From such distributions, it is possible to derive the theoretical mean values of several E or the theoretical $\%E > t$. Some of these values are reported in Table 2 and may be compared with the corresponding experimental values of several sets of reflections to verify whether the structure is **cs** or not.

In this work, for room temperature data, the magnitudes of 82 $hki0$, $hh2\bar{h}l$, $000l$, and $hh2\bar{h}0$ unique electron diffraction intensities were used to calculate normalized structure factors[30] (see eq 1). A Wilson plot of the experimental intensities indicates that the overall isotropic temperature factor is B_{iso} = 0.0 Å^2. This is an often-observed indicator of dynamical scattering (see, for instance, ref 38). Following our previous observations on intensity variation of various reflections verified by continuous tilt measurements of SAED patterns at different goniometer settings (Figures 3 and 4), we assume that observed reflections are influenced by dynamic scattering.[30] Therefore, according to Vainstein,[38] we consider $|F_h| \propto I_h$ as an approximate compensation for dynamical scattering, the relation $|F_h| \propto I_h^{1/2}$ being valid only in the case of kinematic approximation.

The $(hki0)$, $(hh2\bar{h}l)$, $(000l)$, $(h0\bar{h}0)$, and $(hh2\bar{h}0)$ reflections were scaled for every zone and row (e.g., such that $\langle|E_{hki0}|^2\rangle$ = 1.0 for the $(hki0)$ row). The $(hkil)$ and $(h0\bar{h}l)$ reflections were not included in our data set because of bad data quality (their intensities were affected by crystal tilt and local crystal distortions). Calculated values are gathered in Table 2a, suggesting that the observed $(hki0)$, $(hh2\bar{h}l)$, $(000l)$, $(h0\bar{h}0)$, and $(hh2\bar{h}0)$ reflections present a **cs** distribution of intensities.

The above data indicate, according to Table 1, that the possible point group symmetry is *6/mmm* (where all sets are centric). However, in order to further check the validity of this conclusion, the question at this stage is: can the errors on the intensity evaluation be so important as to make a **cs** distribution appear **ncs** or vice versa?

Following Rogers et al.[39] among the different type of errors, we may point out random errors, systematic errors relative to intensities, and errors due to paucity of reflections. Relative to systematic errors, e.g., those depending on the experimental methodology to measure intensities, it is shown that this source of error may cause the diffraction distribution of a **cs** crystal appearing as a **ncs** but not vice versa.[40] However, the paucity of considered reflections in some cases may reduce the reliability of information whether some distribution of intensities is **cs** or not.

As an alternative, to confirm the validity of the *6/mmm* point group, we used the "average intensity method" [30,35-37] the results of which depend much less on the paucity of reflections. Wilson[36,37] showed that in every point group the ratio of the average intensity for reflections belonging to zones or rows in relation to the average intensity of the general class $(hkil)$ reflections is a small integer n, called average multiple. For reflections of the general $(hkil)$ class, the following identity holds for every space group: $\langle I_{hkil}\rangle = \Sigma$, where $\Sigma = \sum f_j f_j$ is the sum of the squares of the moduli of atomic scattering functions. On the other hand, we may define a factor S as the "distribution parameter" (as it appears in the distribution of intensities in both **cs** and **ncs**) representing the mean intensity of reflections not systematically absent such that $S = \langle I_{hkil}\rangle = \sum f_i^2$ for the general $(hkil)$ class and $S = \langle I_{na}\rangle = m\sum f_i^2$ $(m \leq 1)$[29] for particular sections and rows. Average multiples of intensities S/Σ corresponding to the 32 point groups for different sections and rows are given in ref 41.

If we consider that $p = S/\Sigma = \langle I\rangle/\Sigma$, where the factor p is called power or statistical weight,[30] tabulated values of p for

(35) Rogers, D. *Acta Crystallogr.* **1950**, *3*, 455-464.
(36) Wilson, A. J. C. *Acta Crystallogr.* **1950**, *3*, 258-261.
(37) Wilson, A. J. C. *Acta Crystallogr.* **1987**, *A43*, 250-252.
(38) Vainstein, B. K; Lobachev, A. N. *Sov. Phys. Crystallogr.* **1956**, *1*, 370-371.
(39) Rogers, D.; Stanley, E.; Wilson, A. J. C. *Acta Crystallogr.* **1955**, *8*, 383.
(40) Parthasavathy, S. *Acta Crystallogr.* **1966**, *21*, 642.
(41) *International Tables for Crystallography*; Kluwer Academic Publishers: Dordrecht, The Netherlands, 1993; Vol. B.

Table 3. Values of p for Trigonal and Hexagonal Point Groups[30]

point group	$hki1$	$hki0$	$hh2\bar{h}1$; $h2\bar{h}h1$; $2h\bar{h}h1$	$hh2\bar{h}0$; $h2\bar{h}h0$; $2h\bar{h}h0$	$h0\bar{h}1$; $0k\bar{k}1$; $h\bar{h}01$	$h0\bar{h}0$; $0k\bar{k}0$; $h\bar{h}00$	0001
$\bar{3}$	1	1	1	1	1	1	3
$\bar{3}$	1	1	1	1	1	1	3
312	1	1	1	1	1	2	3
321	1	1	1	2	1	1	3
$31m$	1	1	2	2	1	1	6
$3m1$	1	1	1	1	2	2	6
$\bar{3}1m$	1	1	2	2	1	2	6
$\bar{3}m1$	1	1	1	2	2	2	6
$\bar{6}$	1	1	1	1	1	1	6
$\bar{6}$	1	2	1	2	1	2	3
$6/m$	1	2	1	2	1	2	6
622	1	1	1	2	1	2	6
$6mm$	1	1	2	2	2	2	12
$\bar{6}m2$	1	2	1	2	2	4	6
$\bar{6}2m$	1	2	2	4	1	2	6
$6/mmm$	1	2	2	4	2	4	12

Table 4. Average Intensity Data for Several Groups of Reflections for the MCM-22 Structure

	ideal values			
	$6/mmm$	622	$\bar{6}m2$	exptal
$\langle I_{0001}\rangle/\langle I_{hki0}\rangle$	6	6	3	4.1
$\langle I_{0001}\rangle/\langle I_{hh2\bar{h}0}\rangle$	3	3	3	2.73
$\langle I_{0001}\rangle/\langle I_{h0\bar{h}0}\rangle$	3	3	6/4	2.84
$\langle I_{h0\bar{h}0}\rangle/\langle I_{hh2\bar{h}0}\rangle$	1	1	2	1.03
$\langle I_{hh2\bar{h}0}\rangle/\langle I_{hki0}\rangle$	2	2	1	1.05

all point groups help to distinguish between different point groups on the basis of statistical information (see Table 3). For example, we note that the $6/mmm$ symmetry implies one row with $S/\Sigma = 12$, six rows with $S/\Sigma = 4$, and seven zones with $S/\Sigma = 2$.

In our work, scaling of observed intensities of the diffraction spots in each zone was done by using the intensities of $(h0\bar{h}0)$, $(0k\bar{k}0)$, or $(hh2\bar{h}0)$ reflections that are common to all the considered electron diffractograms. Results are listed in Table 4 (compare also with theoretical values of Table 3).

As can be observed, the $6/mmm$ point group symmetry (and also the 622) seems to confirm the theoretical results (Table 4) which are in complete agreement with the independent results of the previous microdiffraction analysis. The experimental statistical average data, although sometimes only roughly approximate to the ideal values, are less likely affected by the paucity of reflections or by anomalous structural features.[35-37]

As we pointed out before, in the course of our statistical analysis of reflection intensities the $6/mmm$ symmetry appears to be correct in both statistical methods (e.g., the "distribution" method where the $6/mmm$ symmetry appears as the only possibility and the "method of averages" where this symmetry seems to be confirmed independently of the paucity of reflections) and the microdiffraction analysis. Hence, we may consider the $6/mmm$ as a most probable symmetry for the MCM-22 structure.

On the other hand, despite the possible structural disorder of the zeolite, the indexing of the X-ray powder diffraction pattern is consistent with P6/*mmm* space group symmetry. Again, it is worth mentioning that the results of an independent refinment based on synchrotron X-ray powder diffraction data[5] also indicate that the *P6/mmm* group is the most probable space group for the MCM-22 structure.

Another interesting point is the following: what would happen if the kinematic assumption ($|F_{\mathbf{h}}| \propto I_{\mathbf{h}}^{1/2}$) were used to interpret our data and, particularly, if the agreement between observed and theoretical intensity distribution statistics (Tables 2a and 4) would be more satisfactory?

In that case, as can be seen from Table 2b, observed $(hki0)$ and $(h0\bar{h}0)$ reflections show **ncs** distribution of intensities; (0001), $(hh2\bar{h}0)$, and probably $(hh2\bar{h}l)$ reflections present a **cs** distribution. Besides the fact that the overall agreement between observed and theoretical intensity distribution statistics is rather poor, the above data indicate (Table 1) that the possible point group symmetry is $\bar{6}m2$ (noncentrosymmetric). On the other hand, the agreement between experimental (observed) and theoretical average intensity data for the $\bar{6}m2$ group is also quite poor (Table 4).

The $\bar{6}m2$ group has $p3m1$ projection plane symmetry along the [0001] orientation.[33] Now, if we assume that $\bar{6}m2$ is the correct point group for the MCM-22 zeolite then the [0001] ZOLZ "ideal" symmetry has to be $(3m)$,[32] e.g., lower symmetry than the $(6mm)$ "ideal" symmetry which is actually observed in our [0001] ZOLZ microdiffraction patterns. Although we cannot exclude this possibility, we think that the $6/mmm$ point group (having $6mm$ projection symmetry) is more consistent with our previous microdiffraction analysis and TEM experimental results.

B. Resolution of the Basal Framework Structure by Electron Crystallography Direct Methods. The determination of the projection framework topology by using direct phasing techniques is based on probabilistic estimates for a linear combination of phases,[27] e.g., the triplet:

$$\phi_{\mathbf{h}1} + \phi_{\mathbf{h}2} + \phi_{\mathbf{h}3} = \phi \qquad (4)$$

which represents a structure invariant phase sum when the Miller indices are $\mathbf{h}_1 + \mathbf{h}_2 + \mathbf{h}_3 = 0$.

In this work, we used 37 unique well-resolved reflections of the $(hki0)$ set, by assuming that $F_{\text{obs}} \propto I_{\text{obs}}$ (implying dynamical contribution to those reflections as indicated[38] by $B_{\text{iso}} = 0.0$ Å^2 extracted from the Wilson plot of the experimental intensities). The consequences of this assumption on the final potential map of the structure will be discussed later.

The calculated E_h values were scaled such that $\langle |E_{hki0}|^2 \rangle = 1$. After averaging this in a descending hierarchy, $16|E_{\mathbf{h}}| \geq 0.7$ were used to generate Σ_1 and Σ_2 triplet phase invariants with large enough A_1 and A_2 values so that ϕ could be correctly predicted.

No preliminary assumptions were made about the molecular geometry of the framework topology, only assuming that the framework structure has a centrosymmetric $p6mm$ projection symmetry. After analyzing 42 high-probability Σ_2 triplets we assigned phases to a basis set of 10 $hki0$ reflections (see Table 5). Those reflections extend to $\sin\theta/\lambda \leq 0.211$, e.g., up to 0.237 nm maximum resolution, a value well below the expected T−T distance in zeolites (0.29 nm).[42]

The phase determination progresses as follows: looking through the list of high probability Σ_2 triples, we assigned algebraic quantities ($a-e$ in Table 4) which permuted through $0,\pi$ to five different reflections. Hence, $2^5 = 32$ different potential maps were calculated. We tried to choose the "best" E-map on the basis of the known structural characteristics of the MCM-22 structure. In fact, as we pointed out before, according to previous catalytic measurements and from zeolite chemistry data,[2,3] large 10- or 12-member ring pores and T−T distances of about 0.3 nm are expected to be visualized along the [0001] direction in the considered "correct" solution.

All but one calculated E-maps were discarded on the basis of their bonding geometry. In the "correct" E-map projection

(42) Liebau, F. *Structural Chemistry of Silicates*; Springer Verlag: Berlin, 1985.

Table 5. Direct Phase Determination for (*hki*0) Reflections of the MCM-22 Zeolite (Only the ϕ_1 Phase Set Corresponds to the Correct Framework Base Model)

algebraic unknowns:
$\phi_{10\bar{1}0} = a$; $\phi_{31\bar{4}0} = b$; $\phi_{11\bar{2}0} = c$; $\phi_{22\bar{4}0} = d$; $\phi_{50\bar{5}0} = e$

Σ_2- Triple Invariants (Largest Positive Values of A_2)

		conclusion
$\phi_{20\bar{2}0} + \phi_{-(31\bar{4}0)} + \phi_{11\bar{2}0}$		$\phi_{20\bar{2}0} = b - c$
$-b$	c	
$\phi_{30\bar{3}0} + \phi_{-(50\bar{5}0)} + \phi_{20\bar{2}0}$		$\phi_{30\bar{3}0} = (c + e) - b$
$-e$	$b - c$	
$\phi_{33\bar{6}0} + \phi_{-(31\bar{4}0)} + \phi_{-(02\bar{2}0)}$		$\phi_{33\bar{6}0} = c - 2b$
$-b$	$c - b$	$\phi_{20\bar{2}0} = \phi_{02\bar{2}0}$ as equivalent
$\phi_{32\bar{5}0} + \phi_{-(33\bar{6}0)} + \phi_{01\bar{1}0}$		$\phi_{32\bar{5}0} = c - (a + 2b)$
$2b - c$	a	$\phi_{10\bar{1}0} = \phi_{01\bar{1}0}$ as equivalent
$\phi_{21\bar{3}0} + \phi_{-(\bar{1}4\bar{3}0)} + \phi_{\bar{3}300}$		$\phi_{21\bar{3}0} = 2b - (c + e)$
$-b$	$c + e - b$	$\phi_{\bar{3}300} = \phi_{30\bar{3}0}$ and $\phi_{\bar{1}4\bar{3}0} = \phi_{31\bar{4}0}$ as equivalents

Correct Solution for $a = c = e = \pi$, $b = d = 0$, ϕ_1 Phase Set

*hki*0	*E*	ϕ_1	ϕ_2
$10\bar{1}0$	2.14	π	π
$20\bar{2}0$	1.34	π	π
$30\bar{3}0$	1.26	0	π
$11\bar{2}0$	0.91	π	0
$22\bar{4}0$	1.41	0	π
$31\bar{4}0$	3.59	0	π
$32\bar{5}0$	1.16	0	π
$50\bar{5}0$	1.16	π	0
$33\bar{6}0$	1.57	π	0
$21\bar{3}0$	0.83	0	0

shown in Figure 8a (corresponding to ϕ_1 phase values of Table 5) we can recognize a large 12-fold ring of 0.72 nm diameter (predicted in ref 2) and T−T distances ~0.3 nm. This image has been calculated with the aid of CRISP software[43] and shows atomic densities as arbitrary grey levels; the same projection, represented (Figure 8b) as electron density values (of arbitrarly scale), shows again this 12-fold ring which can be assigned to the observed 0.72 nm cavity.

Inside the 12-fold ring, atomic density in the form of the hexagonal ring is observed (Figure 8a). The same density can also be appreciated in Figure 8b, although peak maxima are quite badly defined. In fact, the existence of this "inner" ring of density comes from the projection of the "upper" layer structure level as we shall later show in our discussion.

It seems quite improbable that this "inner" ring is found at the same level as the 12-fold aperture. If it were, the observed T−T distances between the adjacent "inner" 6-fold ring and the "outer" 12-fold ring should be shorter than the typical T−T distances (0.3 nm) in zeolites, as long as the "inner" hexagonal ring must have a radii comparable to the T−T distance.

On the other hand, the existence of the observed large 12-fold aperture seems probable since the largest voids in zeolite structures tend to occupy the positions of highest symmetry of the space group of the framework[45] and, consequently, it is logical that the centers of the largest voids do coincide with the 6-fold axes.

On the basis of the above discussion, we may propose as the most probable connectivity between 12-fold pores the one that is shown in Figure 8a,b. On the other hand, although is probable that not all observed T-sites are exactly at the same layer level, we think that Figure 8c satisfactorily represents the atomic density at a layer section containing the large 12-fold rings. Density values inside the 12-fold rings have been neglected as they were considered to emerge from the projection of "upper" layer levels as we shall later see in the discussion in relation to Figure 10b.

Figure 8d shows an example of considered "false solution" (although good from the electron crystallography point of view) corresponding to the ϕ_2 phase set. The pore opening appears significantly larger than 0.72 nm and the possible T−T distances seem heavily distorted.

The observed framework connectivity seen on Figure 8a−c, is further justified if we take into account the large dimension of the 12-fold main channels and the *p6mm* framework projection symmetry (Figure 9a). The 12-fold ring is supposed to be large (0.72 nm) and supporting the mirror operations of the *p6mm* plane group. Then, adjacent 12-fold rings are interconnected in their respective nearest T atoms by a T−T distance of ~0.3 nm. If we take into account the restriction of typical T−T distances (0.3 nm) in zeolites and that 4-, 5-, and 6-fold rings are commonly observed (or proposed) in basal connectivities of these zeolites[42] and also that 8-fold rings do not seem to be present according to our catalysis measuments,[2,3] two possible basal framework arrangements for the MCM-22 structure compatible with the *p6mm* symmetry can be suggested (Figure 9a,b). The model of Figure 9a is in agreement with the proposed framework in Figure 8a,b.

C. Structure Analysis of the 3D Framework Structure by Electron Crystallography Direct Methods. As becomes evident from our analysis of the MCM-22 structure, we made use only of (*hki*0) reflections to resolve the basal framework topology, assuming that these mainly contribute to the electron density of the basal plane. On the other hand, to reveal the 3D framework topology, we need at least one $(1\bar{1}00)$ and/or $(11\bar{2}0)$ E-map projections.

Unfortunately, corresponding $(hh2\bar{h}l)$ or $(h0\bar{h}l)$ SAED patterns are difficult to obtain because of the very pronounced crystal texture along the [0001] projection, and on the other hand, when they are obtained they are of quite bad quality for precise intensity measurements as they are usually affected by local crystal tilts and rapid radiation damage.

The whole intensity contribution of the (000*l*) reflections—compared to the (*hki*0) reflections—seems to be very important (see Table 4). Assuming that there are few interactions between (000*l*) and the most intense (*hki*0) reflections and as long as any two intense spots of a (000*l*) reciprocal row are separated by a low intensity node (see Figure 4), we consider that, according to ref 17, (000*l*) reflections can be used by themselves, e.g., such reflections have large enough A_2 values to reliably estimate the phase of the triplet invariant. The results of this analysis are shown in Table 5 after examining the highest probability Σ_1 and Σ_2 triplets. Two solutions, called A and B, with different phase sets are proposed.

In order to choose between the two possible phase sets and further resolve the 3D structure, we calculate E-maps down to the $[11\bar{2}0]$ direction combining (000*l*) and (*hki*0) data. Two E-maps were calculated (Figure 10a,b) by considering (*hki*0) phases corresponding to the "correct" base framework model (Table 5, ϕ_1 values) and each one of the two possible A and B (000*l*) phase sets (Table 6). Again, the correct map can be chosen on the basis of the known characteristics of the MCM-22 structure. From our catalytic measurements,[2] we are aware that the structure has a system of large interconnecting 12-fold or 10-fold channels of size ranging from 0.72 to 0.59 nm, respectively.

Moreover, it turns out that only one of the two maps (Figure 10b) has a good density envelope and could be chosen a priori on the basis of "peakiness".[45] Unfortunately, in the chosen

(43) Hovmoller S. *Ultramicroscopy* **1992**, *41*, 121−135.
(44) Brunner, G. O. *Zeolites* **1990**, *10*, 612−614.
(45) Stanley, E. *Acta Crystallogr.* **1986**, *A42*, 297−299.

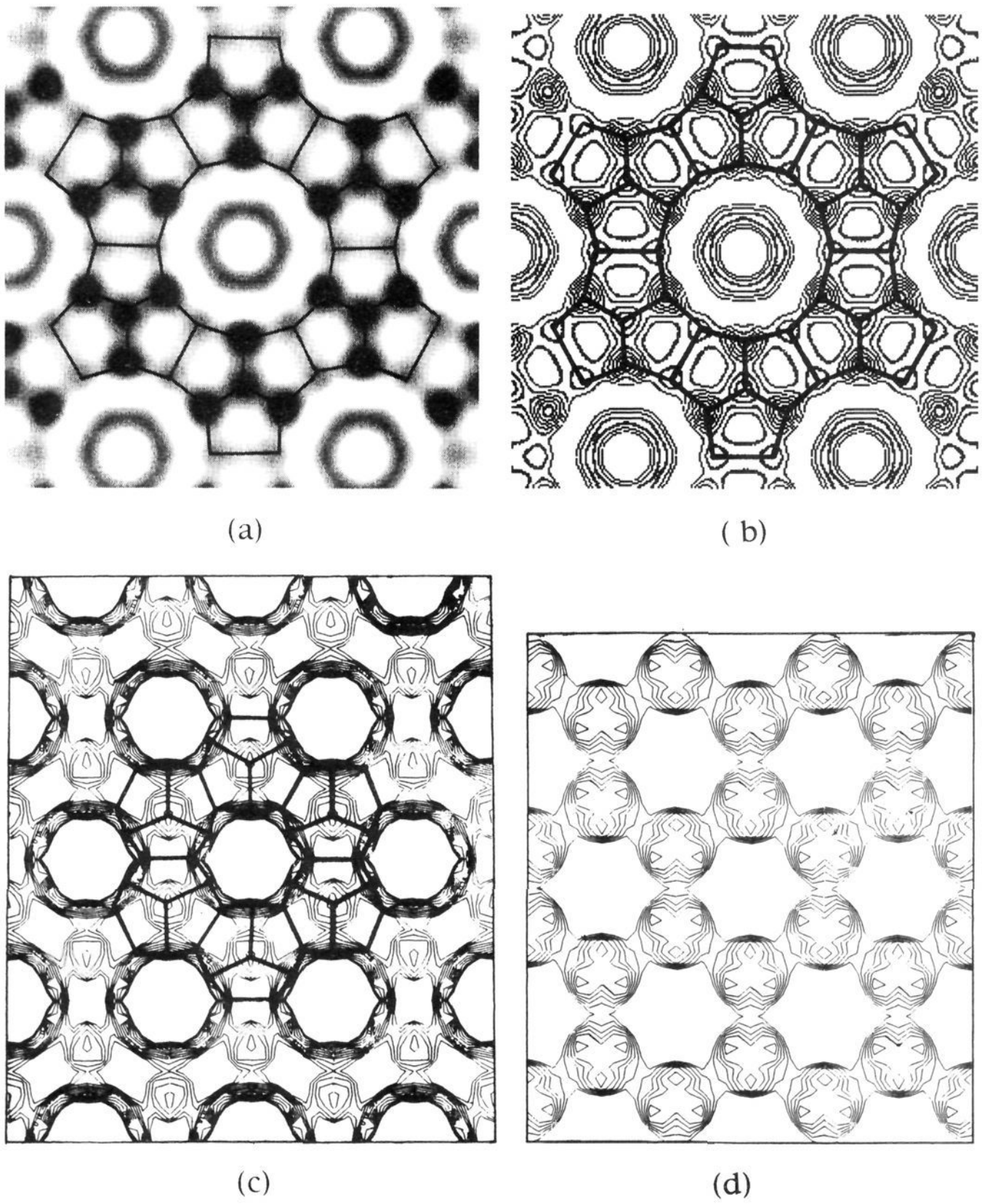

Figure 8. E-maps for MCM-22 zeolite along the [0001] direction The structure is identified from chemical knowledge of the bonding geometry. (a) [0001] projection, "correct" choice of phases: large 12-fold pores and the connectivity between them can be readily identified. (2 × 2) cells are represented with $a = b = 1.43$ nm. (b) Same as part (a) projection visualized as electron density levels (arbitrary values). (c) Proposed basal layer section containing the 12-fold ring apertures (4 × 4) cells. (d) Combination of phases in the multisolution determination leading to the wrong geometry.

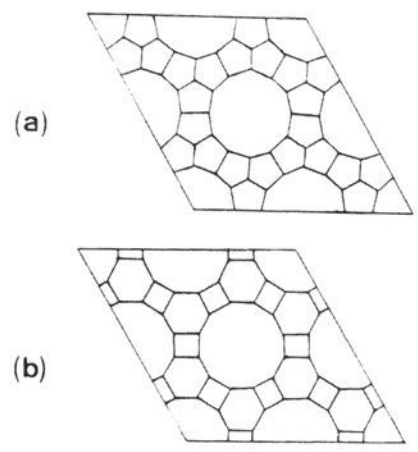

Figure 9. Two possible models (a and b) showing the connectivity between large 12-fold apertures for the MCM-22 structure. Only T atoms are shown.

"correct" E-map, atomic details are roughly resolved, presumably because of the low number of considered reflections in the structure determination. However, despite the poor resolution in the potential map of Figure 10b, very interesting structural details can be revealed: The 12-fold ring aperture

Table 6. Phase Assignments for MCM-22 Structure Analysis of the (000l) Reflections

Σ_1- Triples (Positive Values of A_1)	
$\phi_{0002} + \phi_{0002} + \phi_{0004} = 0$ for $\phi_{0002} = 0,\pi$ then $\phi_{0004} = 0$	
$\phi_{0002} + \phi_{0002} + \phi_{0004} = 0$ for $\phi_{0002} = 0,\pi$ then $\phi_{0008} = 0$	
Σ_2- Triples (Largest Positive Values of A_2)	
$\phi_{0006} + \phi_{0002} + \phi_{0004} = 0$	for $\phi_{0002} = 0$ then $\phi_{0006} = 0$
	for $\phi_{0002} = \pi$ then $\phi_{0006} = \pi$
$\phi_{0008} + \phi_{0006} + \phi_{0002} = 0$	for $\phi_{0002} = 0$ then $\phi_{0006} = 0$
	for $\phi_{0002} = \pi$ then $\phi_{0006} = \pi$
$\phi_{00010} + \phi_{0008} + \phi_{0002} = 0$	for $\phi_{0002} = 0$ then $\phi_{00010} = 0$
	for $\phi_{0002} = \pi$ then $\phi_{0006} = \pi$
two possible solutions:	(A) $\phi_{0004} = \phi_{0008} = \phi_{0006} = \phi_{00010} = \phi_{0002} = 0$
	(B) $\phi_{0004} = \phi_{0008} = 0$, $\phi_{0002} = \phi_{0006} = \phi_{00010} = \pi$

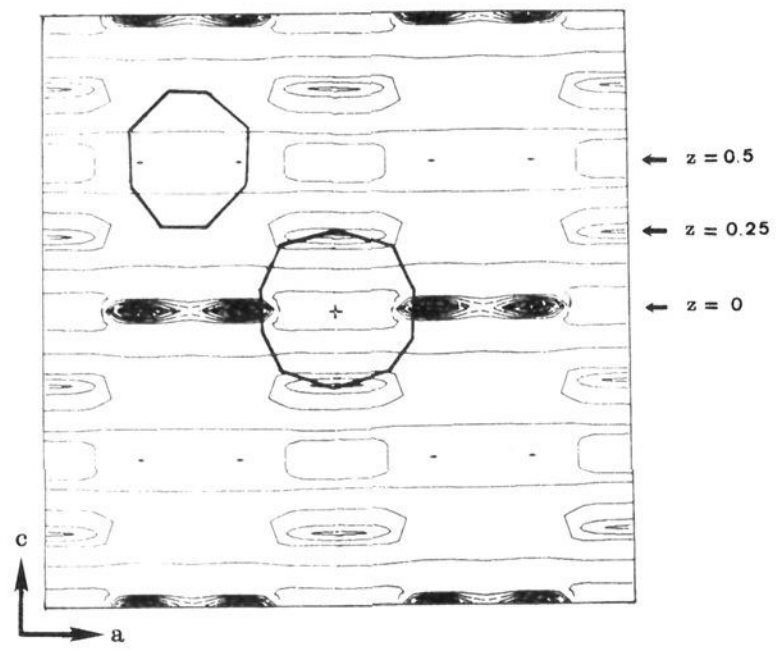

Figure 10. E-maps for the MCM-22 zeolite [11$\bar{2}$0] projection calculated by combining ϕ_1 phase values (Table 4) with: (a) using (000l) (A) phase set (Table 6) and (b) "correct" map using (000l) (B) phase set (Table 6). Map origins are at the center and (4 × 4) cells are represented. The proposed model in ref 5 for big interlayer and intralayer supercages is superimposed in both maps for comparison.

seen in the projected basal framework (Figure 8a,b) is now seen at the center of the (11$\bar{2}$0) E-map at $z = 0$, bounded by a pair of atomic densities (at $z = 0$) corresponding to a T−T bonding. On the other hand, it seems that the 12-fold ring aperture in the basal plane does not form a "free" 12-fold tunnel parallel to the c axis. In fact, strong atomic density at $z = 0.25$ indicates that the walls of the possible 12-fold tunnel parallel to the c axis significantly approach, forming probably a large supercage cavity (Figure 10b). Those walls lead to a narrow (probably 6-fold) aperture which projected down on the (0001) plane is visualized as the observed "inner" ring in Figure 8a,b.

According to this interpretation, now the occurrence of atomic density regions inside the 12-fold apertures in the [0001] projection (Figure 8a,b) is better understood, as we pointed out before. This supports the interpretation that Figure 8c satisfactorily represents atomic density values of the layer containing the 12-fold apertures (besides some small possible 3-D modulation of T sites in the 12- and 5-fold rings as frequently occurs in zeolites[42]).

In conclusion, according to the (11$\bar{2}$0) E-map of Figure 10b, the tunnel parallel to the c axis leading to a 12-fold aperture in the basal plane seems to have a 2D sinusoidal variation along the c direction.

Discussion

In relation to the previous discussion about the proposed projected framework model of the MCM-22 structure, it seems of interest to further discuss the Moiré pattern interpretation (Figure 7, bottom inset). In fact, it appears now that the straightforward interpretation of this Moiré pattern in terms of projected framework topology is not as fortuitous as it was thought to be (see previous comments). As can be observed, if one looks carefully into the white dot pattern within the Moiré supercell, large symmetrical white rings appear to be bounded by smaller pentagonal rings, showing that way a striking similitude with the proposed framework connectivity model of Figure 8a,b.

On the other hand, it is of interest to discuss and compare our electron crystallography direct phasing results with the MCM-22 framework model proposed by Leonowitz et al.[5] after extensive X-ray synchrotron data analysis.

Our work leads to the same framework connectivity model between the large 12-fold pores as the most probable for the MCM-22 structure as in ref 5. However, some slight difference can be appreciated (compare with Figure 3 of ref 5) about the relative orientation of the "inner" hexagonal ring—which is projected to the basal plane from the "upper" level structure layer—in relation to the 12-fold aperture.

We think that such a discrepancy may be due to the fact that some of the phase values of the ϕ_1 phase set (one ot two) probably are not correct (possibly because of some incorrectly predicted $\sum_2$ phase sums). In fact, is quite frequent that some phases are incorrectly assigned during the process of direct phase determination, but this normally only slightly affects the final results.[10,15,16,46] Concerning the 3-D structure, the existence of large supercages having ($4^2 5^8 10^2$) topology is shown in ref 5. Those supercages stack one above the other along the c axis direction through double 6-fold rings, the supercage diameter being defined by a 12-member ring. Such stacking arrangement of supercages leads to the formation of sinusoidal intralayer channels with access through elliptical slightly folded 10-ring apertures. There is no communication between the interlayer supercage and the intralayer sinusoidal channel.

The proposed model of the two cavities, according to Figure 2 of ref 5, is superimposed in Figure 10a,b. Given the low resolution of the (11$\bar{2}$0) E-map (because of the low number of considered reflections in structural determination), the detailed form and even the existence of those cavities can only be inferred in the (11$\bar{2}$0) E-map of Figure 10b. However, despite the low number of reflection data used, important information such as the sinusoidal variation along the c direction of the 12-fold pores is already inferred from the E-map of Figure 10b.

An obvious question arising at this stage of potential map interpretation is: how our assumption about the dynamical scattering contribution in all reflections could influence (scramble or even change) structural characteristics in the E-map at the point that structure determination might be misleading?

Early work on the ferroelectric heavy atom structure of $BiFeO_3$[47] shows that although the considered reflections in the structure analysis were influenced, to some extent, by dynamical scattering, independently by the formula used to convert I_{obs} to F_{obs} (e.g., $I_{obs} \sim F_{obs}^2$ for kinematic or $I_{obs} \sim F_{obs}$ for dynamic scattering), the structure refinement factor $R(\%)$ residuals are minimum, in both cases, at about the same Bi−Fe distances. In fact, despite the influence of dynamical interaction on reflec-

(46) *Direct Methods of Solving Crystal Structures*; NATO ASI Series; Shenk, H., Ed.; Plenum Press: New York, 1991.

(47) Tomashpol'skii, Y. Y.; Venevtsev, Y. N.; Zhdanov, G. S. *Sov. Phys. Crystallogr.* **1965**, *9*, 715−720.

tions, even displacement of light atoms (oxygens) could clearly appear in the E-map.

Cowley[48] also showed that, even using uncorrected intensities in structure determination, it is possible to estimate the coarser features of the structure of dicetyl ($C_{32}H_{66}$) (e.g., C−C atoms). Recent work by Dorset[10] on the thiourea structure assuming both "kinematical" ($I_{obs} \sim F_{obs}^2$) or only "dynamical" formula ($I_{obs} \sim F_{obs}$) for scattering of intensities led to essentially the same potential maps (unless for some distortions on both distances and angles when the "kinematical" formula was used).

In fact, even if dynamical scattering is observed to change measured values of F_{obs} and thus E_{obs} it is apparent that this data perturbation may preserve kinematical phase information. Though this may seem quite surprising at first, satisfactory explanations now are beginning to emerge and are extensively described elsewhere.[49] According to those explanations, one of the most convenient ways to carry out a calculation of n-beam dynamical scattering is the slice method of Cowley and Moodie.[50,51]

In order to simulate (hk) dynamical intensities the phase grating approximation can be written in the form

$$F^{dyn}_{hk} = i\sigma F_{hk} - (\sigma^2/2!)F_{hk}*F_{hk} - (i\sigma^3/3!)F_{hk}*F_{hk}*F_{hk} + \ldots \quad (5)$$

where σ is an interaction term;[49] details about the validity of this approximation are further described in ref 49. According to ref 49, it is shown that the preservation of kinematical phase information in these dynamical intensities may be due to the dominance of $F_{hk}*F_{hk}$, $F_{hk}*F_{hk}*F_{hk}$ etc. terms in the phase grating series. As long as this perturbation is not too pronounced, phase information is preserved, by analogy to the Sayre equation,[52] by the convolution operation even though the magnitude of the structure factors might be changed.

In other words, that this data perturbation can be somewhat tolerated in direct-phase determination it is not too surprising as correct structure maps depend on correct phases much more sensitively than on the absolute beam amplitudes.[11,16,53]

Therefore, the essential features of the framework structure of MCM-22 (revealed in the E-maps of Figures 8b and 10b) are essentially correct besides the dynamical scattering contribution to all reflections. Hence, having a correct basic building model, further structure details may be revealed, locating lighter atoms in succesive potential maps.[54]

Up to now, despite the very promising results of electron crystallography on early structure determinations in layer silicate minerals and in the complex aluminosilicate structure of staurolite, no attempt has been made to resolve zeolite frameworks. It seems to be demonstrated, as far as more experience is gained with electron crystallography,[8−26] that it presents a reasonable alternative to many materials poorly crystallized or available only in powder form.

In our work, the ab initio analysis of the MCM-22 zeolite with electron diffraction data leads to correct predictions concerning the point and the space group, the basal framework topology, and the basic features of the whole 3D structure. In spite of the fact that SAED data cannot be as accurate as single crystal XRD refinments, this work shows that ab initio analysis of the zeolite structure with electron crystallography methods may be possible, permitting at least the construction of an essentially correct basic building model.

Conclusion

Direct phasing techniques from electron diffraction data and a parallel independent X-ray synchrotron study of the new MCM-22 zeolite structure lead to the same results. To our knowledge, this is the first time that electron crystallography techniques have been applied in zeolite compounds. Zeolite structures present many problems to structure determination and very often only powder XRD data or TEM images are available for structure determination.

Energy minimization model building programs and time-consuming extensive refinements are often needed to determine new zeolite structures.[55] On the other hand, high resolution electron microscope images are quite hard to obtain because zeolites are highly beam-sensitive materials. Recently,[56] a newly developed procedure for recording low-dose images from zeolites with a resolution better than 0.2 nm using a commercial CCD camera has presented an advance in this field.

Obviously, as is shown in this paper, electron crystallography may present an interesting alternative to the ab initio model building for zeolite structures. SAED patterns are easier to obtain comparable to high resolution images. On the other hand, as we observe in this work the paucity of reflections and the existence of dynamical scattering is not deleterious for, at least, an approximate crystal structure determination from SAED data.[8,10,11,47,48] Only when accurate bond distances and angles are required must attention be paid to the geometry of data collection, crystal thickness effects, and other factors.[14]

Acknowledgment. Financial support by C.I.C.Y.T. (Spain) through Research Projects No. MAT91-0331 and MAT93-0207 is acknowledged. We thank Dr. Amador U. (X-Rays Lab., UCM) for writing a Fourier map calculation program and M. Perez and J. M. Aznar (C.S.I.C., Optics Department) for technical assistance.

JA943685+

(48) Cowley, J. M.; Rees, A. L. G.; Spink, J. A. *Proc. R. Soc.* **1951**, *64*, 609−625.
(49) Dorset, D. L.; McCourt, M. *Electron Crystallography, Transactions* **1992**, *28*, 105−113.
(50) Cowley, J. M. *Diffraction Physics*, 2nd ed.; North Holland: Amsterdam, The Netherlands, 1981; pp 236−238.
(51) Cowley, J. M.; Moodie, A. F. *Acta Crystallogr.* **1959**, *12*, 360−367.
(52) Sayre, D. *Acta Crystallogr.* **1952**, *5*, 60.
(53) Ramachadran, G. N.; Srinvasan, R. *Fourier Methods in Crystallography*; Wiley Interscience: New York, 1970; pp 62−67.
(54) Dorset, D. L.; McCourt, M. P.; Fryer, J. R.; Tivol, W. F.; Turner, J. N. *MSA Bull.* **1994**, *24*, 398−404.
(55) McCusker, L. B. *Acta Crystallogr.* **1991**, *A47*, 297−313.
(56) Pan, M.; Crozier, P. A. *Ultramicroscopy* **1993**, *52*, 487−458.